An Analysis of Subtidal Current Fluctuations in the Middle Atlantic Bight[1]

HSIEN WANG OU[2] AND ROBERT C. BEARDSLEY

Woods Hole Oceanographic Institution, Woods Hole, MA 02543

DENNIS MAYER

Atlantic Oceanographic and Meteorology Laboratories, NOAA, Miami, FL 33149

WILLIAM C. BOICOURT

Chesapeake Bay Institute, The Johns Hopkins University, Baltimore, MD 21218

BRADFORD BUTMAN

U.S. Geological Survey, Woods Hole, MA 02543

(Manuscript received 28 November 1980, in final form 1 July 1981)

ABSTRACT

Subtidal current fluctuations in the Middle Atlantic Bight are examined from current-meter data collected in 1975 and 1976. Spectral analysis provides evidence for both locally wind-forced response and free waves that propagate downshelf[3] which are not correlated with the local wind. A simple empirical model has been constructed to fit two linearly independent plane waves to the observed current spectra. Application of the model to the current data obtained at a pair of stations in the New York Bight during the period of 26 October 1975 to 4 April 1976 indicates that the two waves propagate in opposite directions along the coast, and with the additional evidence from rotary-coefficient calculations, it is suggested that they correspond to the forced and free waves speculated upon earlier. The noise level is a free parameter in the model and is determined by adjusting the phase speed of the forced wave to the translation speed of the observed wind field. This gives a 526 km day^{-1} phase speed for the free wave, and the forced wave, free wave and noise compose ~41, 39 and 20% of the total variance.

1. Introduction

Wind is known to cause much of the subtidal current variability over the continental shelf in the Middle Atlantic Bight (Beardsley and Boicourt, 1981). Although momentum is imparted to the water column locally, it also can be carried downshelf by coastally trapped waves. At a fixed location, the water motion therefore can consist of both a component forced by the local wind and a component that has traveled there from the upshelf direction. The simple shelf-wave model of Gill and Schumann (1974) has very elegantly illustrated this point. Observationally, the existence of both components in the Middle Atlantic Bight has been documented in coastal sea level records by Noble and Butman (1979) and Wang (1979). In a rather extensive analysis, Wang (1979) has found that the locally wind-forced response dominates from Cape Cod to Cape May, while a southward phase propagation of 600 km day^{-1} was observed between Cape May and Cape Hatteras which was not correlated with the local wind. The regional variation of the relative importance of the two components was ascribed to the different meteorological conditions in the two areas and the sharp bending of the coastline at the mouth of the New York Bight. Since both the forced and free waves contribute in a varying degree to the observed motion, the interpretation of data in terms of one single plane wave can at times be misleading. We therefore carry the analysis one step further to interpret the observed current fluctuations in terms of two plane waves and obtain a quantitative estimate of the relative importance of each component.

The data set considered in this analysis is described in the next section, followed in Section 3

[1] WHOI Contribution No. 4710.

[2] Present affiliation: Lamont-Doherty Geological Observatory of Columbia University, Palisades, NY 10964.

[3] In this presentation, downshelf and upshelf will refer to the directions that are in and opposite to the direction free shelf waves propagate. In the Middle Atlantic Bight, downshelf is toward the southwest.

0022-3670/81/101383-10$06.50

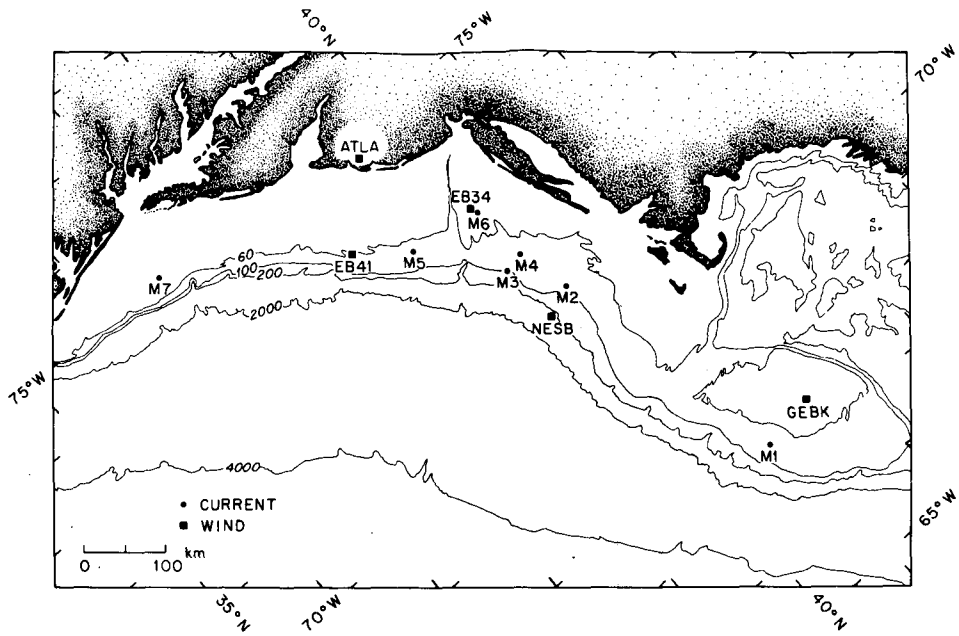

FIG. 1. Bathymetric map of the Middle Atlantic Bight showing the locations of the moored array and the meteorological stations. Isobath depths are in m.

by a local spectral analysis to examine the forced response. A non-local spectral analysis is presented in Section 4 that provides evidence for the existence of free waves. In Section 5, a simple empirical model is constructed to fit two plane waves to the observed current spectra. More discussion of the model and its application follows in Section 6.

2. The data set

During 1975 and 1976, several research groups conducted a moored-array experiment in the Middle Atlantic Bight. We show in Fig. 1 the locations of the particular current-meter moorings (solid squares) and meteorological stations (solid circles), the data from which will be discussed in this paper. The moorings have been numbered sequentially from north to south, and from deep water shoreward. The current meters on the same mooring will be identified by a second digit that increases with the depth of the instrument. Some relevant information about the data is summarized in Table 1, and the record lengths are shown schematically in Fig. 2. The current-meter data have been rotated to align with local isobaths, the orientation of which is indicated in Table 1. The wind was measured at Atlantic City (ATLA) and the NOAA environmental buoys EB41 and EB34, and was estimated for sites at the New England shelf break (NESB) and Georges bank (GEBK) from six-hourly synoptic surface-pressure charts. Wind stress has been computed from the wind vector using the quadratic drag law and a constant drag coefficient of 1.5×10^{-3}. Both current and wind-stress data have been low-pass filtered to remove tidal and shorter period fluctuations. The resulting time series have then been resampled at 6 h intervals for the analysis.

We show in Fig. 3 a segment of some time series of wind stress and alongshore currents. Consistent with the synoptic character of the cyclones that

TABLE 1. A composite table summarizing the information concerning the data used in the analysis.

Mooring I.D.	Latitude (°N)	Longitude (°W)	Water depth (m)	Instrument type	Instrument depth (m)	Topography orientation (deg from Z)	Sponsor
M1	48°51′	67°24′	85	VACM	15, 45, 75	32	USGS
M2	40°22′	71°12′	83	VACM	38, 73	23.2	NSF
M3	39°59′	71°57′	83	VACM	38	32.4	NSF
M4	40°12′	72°0′	66	Aanderaa RCM4	20, 40, 60	45	MESA (NOAA)
M5	39°16′	73°1′	70	Aanderaa RCM4	19, 39, 59	45	MESA (NOAA)
M6	40°7′	72°55′	47	Aanderaa RCM4	19, 39	45	MESA (NOAA)
M7	39°50′	75°2′	35	VACM	10, 20, 30	90	NSF

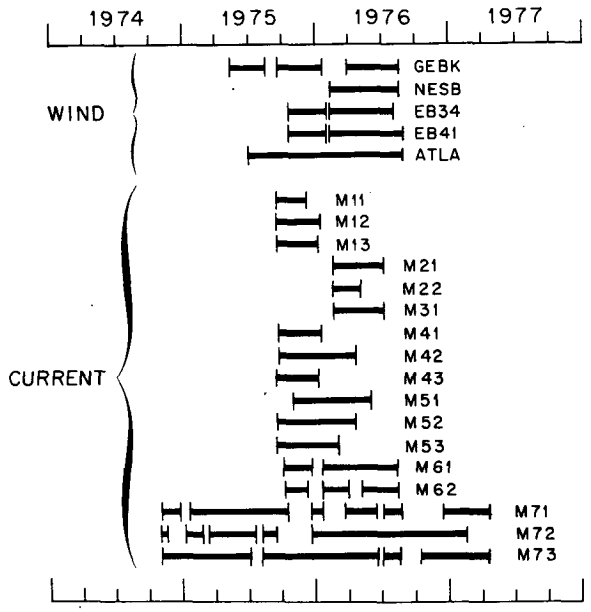

FIG. 2. A diagram showing the duration of the data.

dominate the region in winter time (Mooers *et al.*, 1976; Beardsley and Boicourt, 1981), the wind-stress data from the different stations are similar and hence only the wind-stress data from EB41 are shown. The current time series are characterized by irregular occurrences or events of a few days duration. The more intense bursts of current motion correlate well with one another and clearly are the responses to the similar bursts in the wind stress. But there also are current fluctuations that have no apparent association with the wind stress, suggesting a significant non-locally wind-forced motion.

3. Local analysis

In order to illustrate some common features, we show in Fig. 4 autospectra of wind stress (solid squares) and current (solid circles) computed for two different time periods. The two time periods have been spaced as far apart as our data allow to minimize the dependence of the two records. Since the spectra are inherently red (i.e., the power density increases toward lower frequency), it is not surprising that the spectral shapes for the two different time periods are quite different. But the similarity of the spectral shapes within the same time period, and in particular the concurrence of the spectral peaks between wind stress and current suggests that the more energetic current fluctuations are driven by

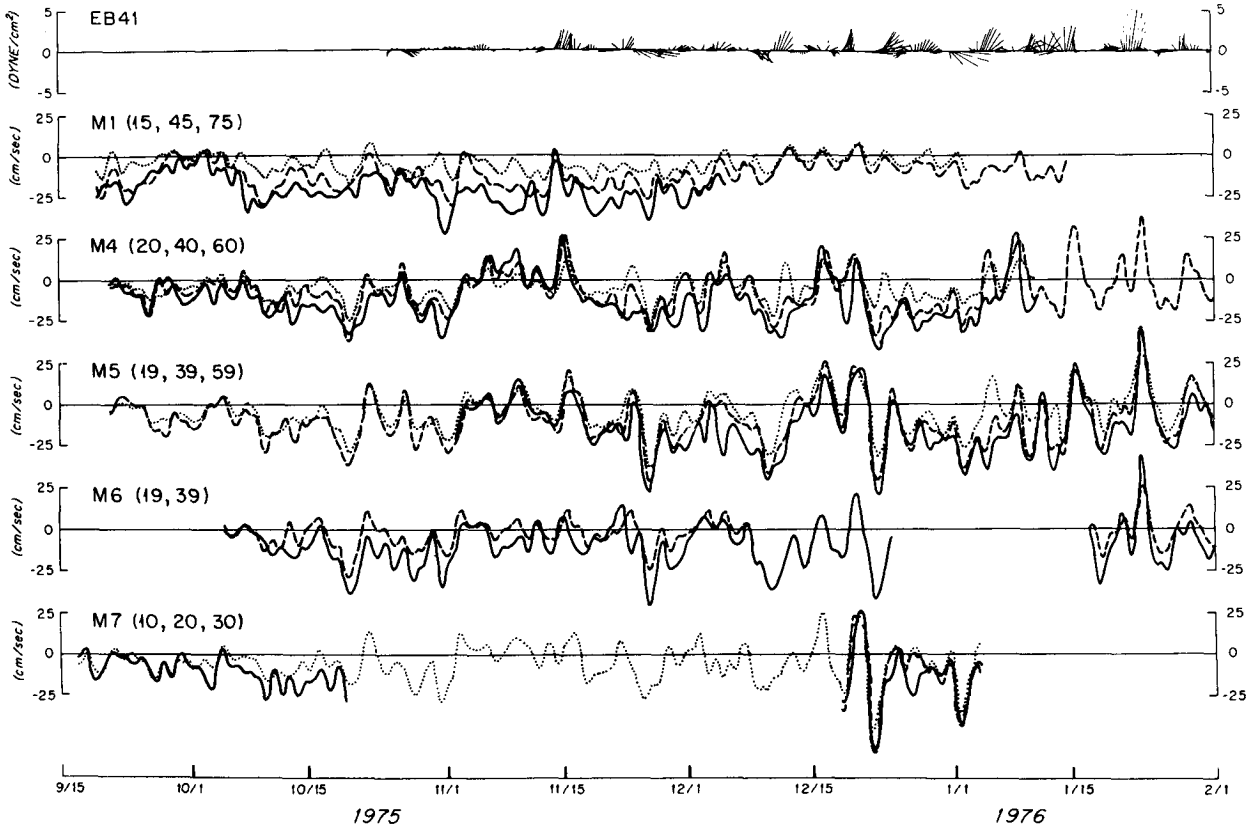

FIG. 3. A segment of some time series of wind stress and alongshore currents. For the current meters on the same mooring, solid, dashed and dotted lines represent the data recorded at increasing depths (indicated in meters in the bracket). For the wind-stress plot, east is in the positive direction, and for the alongshore current data, upshelf is positive.

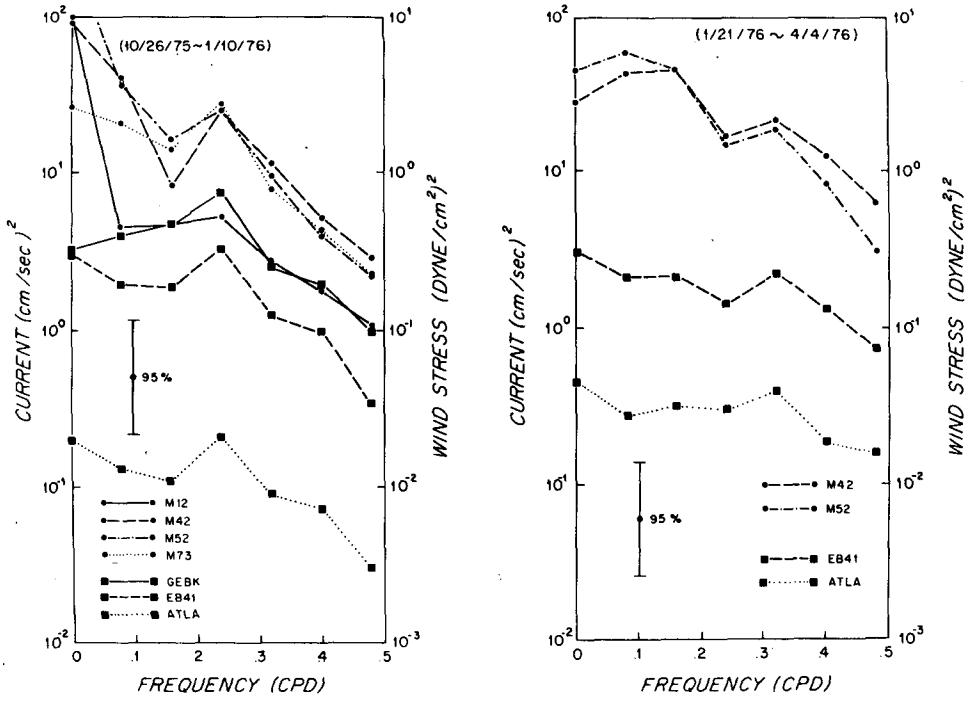

FIG. 4. Autospectra of some of the wind-stress (solid squares) and current-meter (solid circles) data for two different time periods. The spectral estimates have been averaged over six frequency bands.

wind. There is a marked intensification of wind stress offshore and toward the northeast, consistent with the previous analysis of Mooers *et al.* (1976) and Beardsley and Boicourt (1981). During the first period, the wind stress magnitude increases by a factor of 4 offshore from Atlantic City to the environment buoy EB41, and by another factor of 1.5 toward the northeast from EB41 to Georges bank.

For reasons to be discussed in Section 6, we shall present in the following only the analysis using the current-meter data at M42, M52 and wind data at EB41, EB34 and ATLA. The analysis is carried out for the time period of maximum overlap (26 October 1975–4 April 1976) between current and wind data. We show in Fig. 5 the two-sided coherence and phase between alongshore wind stress at EB41 and current at M42. The convention adopted here is such that series 2 lags series 1 when the phase is negative in the clockwise component. The vertical bars indicate the 95% confidence interval, and the dashed lines in the phase diagram represent a time lag of 10 and 20 h, respectively. Except for the zero-frequency estimate, the coherence is significant, and the current lags the wind by a time of order of half a day. Similar calculations carried out for the other current data indicate that the picture shown here in Fig. 5 is fairly representative. For this particular current record at M42, the time lag for the clockwise component is smaller than that for the counterclockwise component, implying a clockwise veering of the major axis of the current ellipse from the local isobath. The low coherence at zero frequency is consistent with the observation that the mean current goes against the mean wind in this region (e.g., Beardsley *et al.*, 1976), and other driving forces must become important (Scott and Csanady, 1976; Beardsley and Boicourt, 1981).

We also want to point out that although the coherence is well above the significance level, the noise can still make up a major portion of the observed variance. It is trivial to show that for a signal-to-noise ratio of one, true coherence can be as high as 0.7. By calculating the transfer function between the input alongshore wind stress and the output current, we can remove the current signal that is coherent with the wind, and examine the residuals. We plot in Fig. 6 the gain of the transfer function, and the autospectra of the original and residual current motions. Except at zero frequency where there is a large uncertainty, the gain of the transfer function is of order of 10, i.e., a 1 dyn cm^{-2} wind stress would cause a 10 cm s^{-1} current fluctuation. It also is seen that more than half of the total variance cannot be explained by local wind forcing. Are these residual current motions pure noise or are they coherent wave signals that propagate down the shelf? These are the questions we hope to answer in the next two sections.

4. Non-local analysis

In this section, we will present cross-spectrum analysis to examine the coherent traveling signals.

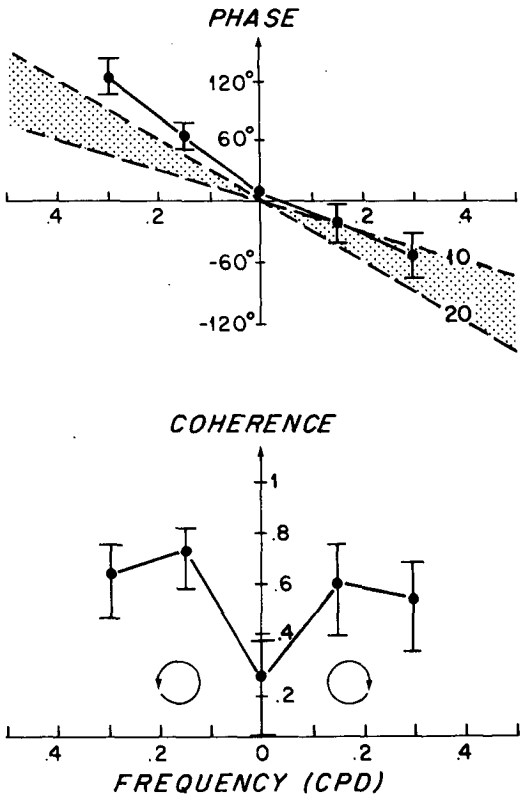

FIG. 5. Two-sided coherence and phase for the alongshore wind stress at EB41 and the current at M42 during the period of 16 October 1975 to 4 April 1976. The estimates have been averaged over 24 frequency bands, and the error bars indicate the 95% confidence interval. The dashed lines in the phase diagram represent time lags of 10 and 20 h, respectively.

To infer the forcing field, we show in Fig. 7 the two-sided coherence and phase of wind stress calculated for the station group of ATLA, EB41 and EB34 forming an approximately equilateral triangle. Since the scale of the wind field is large compared with the separation distances, coherence is high among all three station pairs. The generally negative slope in the phase diagram implies a phase propagation offshore and toward the northeast, consistent with the average path of winter cyclones in this region (Mooers *et al.*, 1976). For a true coherence of 0.8, the 95% confidence interval for the coherence estimate is given by the range (0.56, 0.90), and for the phase estimate is ±24°. Since the phase difference for the station pair ATLA-EB34 is approximately equal to the sum (the dotted line) of the phase differences of ATLA-EB41 and EB41-EB34, the traveling disturbance can be approximated by a single plane wave. We plot in Fig. 8 the direction (°T, clockwise from true north) and the magnitude of the phase speed of this plane wave as a function of frequency. For the 47-frequency-band average shown by the open symbols, the wind field is propagating in the direction 98°T with a phase speed of about 1000 km day^{-1}. The resulting phase difference between M42 and M52 is about 8°.

We show in Fig. 9 the two-sided coherence and phase for the current-meter data at M42 and M52. The high coherence is due to the proximity of the two stations (136 km apart). The phase estimate at zero frequency represents approximately the angle between the two mean currents, which can partly be caused by the uncertainty in estimating local topographic orientation. Adjusted by this angle, the phase difference is small and no definite slope in the phase diagram can be inferred. This lack of a definite temporal relation between the two current records can be accounted for by the presence of both forced and free waves that happen to travel in opposite directions in this region. Similar calculations done for the residual current after removing the signal that is coherent with the alongshore wind are shown in Fig. 10. The coherence is still rather high, implying that the residual current motion has a coherence scale greater than the separation distance between the two stations, and the now apparent negative slope in the phase diagram indicates that the signal

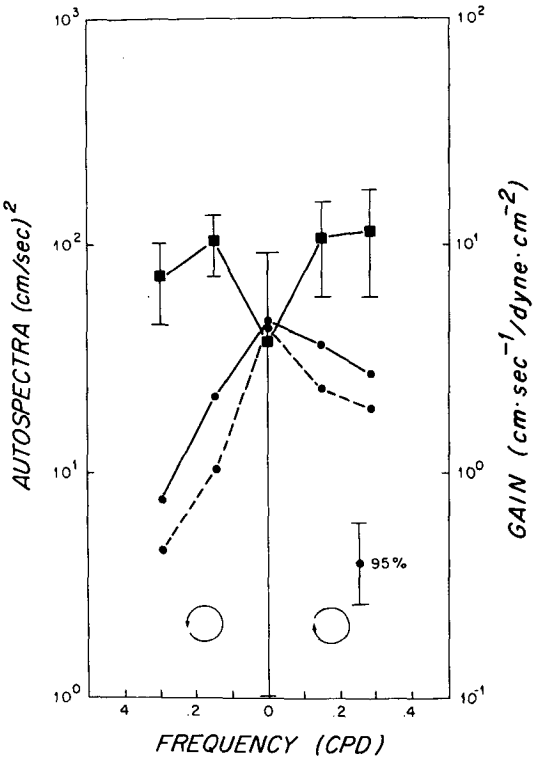

FIG. 6. The gain of the transfer function (solid squares) between the input alongshore wind stress at EB41 and the output current at M42, and the autospectra of the original and the residual current motions at M42 (dots connected by solid and dashed lines, respectively), calculated for the period of 16 October 1975 to 4 April 1976. The estimates have been averaged over 24 frequency bands. The 95% confidence intervals for the gain are shown by the vertical bars attached to each estimate, and for the autospectra are shown by the vertical bars in the lower right corner.

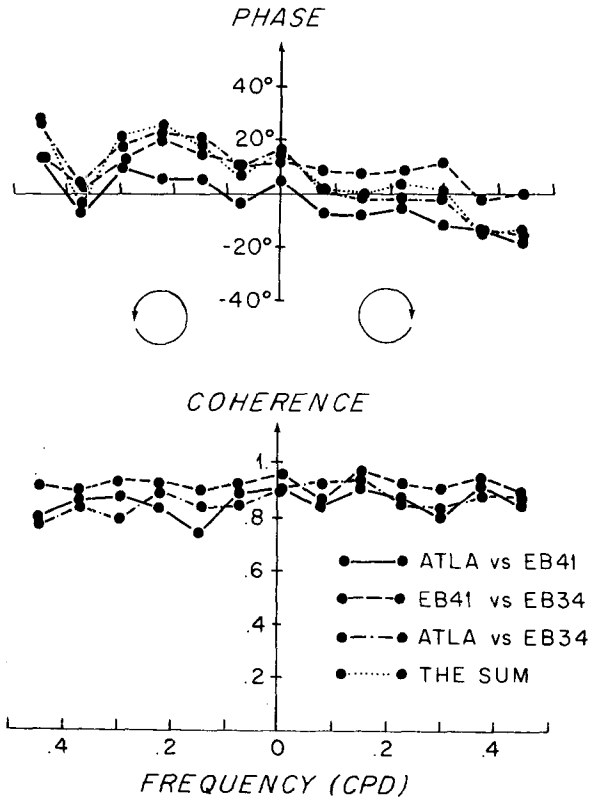

FIG. 7. Two-sided coherence and phase of wind stress, calculated for the station group ATLA, EB41, and EB34 during the period of 16 October 1974 to 4 April 1976. The estimates have been averaged over 12 frequency bands. The dotted line represents the sum of the phase differences of ATLA-EB41 and EB41-EB34.

at M52 is lagging that at M42. For reference, the dashed line represents a nondispersive phase speed of 816 km day^{-1}.

Through spectral analysis, we have presented in the last two sections evidence for both a locally wind-forced response that propagates upshelf and a second (free) wave that propagates downshelf. To assess better the relative importance of these two waves, we will construct next a simple empirical model that fits the current observations by two independent plane waves.

5. An empirical two-wave model

We have constructed an empirical model that fits two plane waves to two current time series measured at two locations separated in the alongshore direction. The model assumes spatial uniformity along the shelf and that the observed motion can be represented by a superimposition of two linearly independent plane waves and noise. For any given noise level, the amplitude and wavenumber of the two waves can be determined in terms of the auto- and cross-spectra of the two current time series as is shown in the Appendix. Although the model is admittedly crude, it does represent a significant improvement over some more conventional practices of interpreting the spectral data in terms of one wave. It also has an advantage over the method of empirical orthogonal functions, which can resolve two primary wave components of comparable amplitude only when they are nearly orthogonal to each other. More waves can be resolved by using more stations, but the algebra becomes much more complicated. Besides, more serious questions arise concerning the spatial uniformity of the wave environment between stations spaced farther apart. For our purpose of differentiating between forced and free waves, the resolution into two waves seems adequate. Since there is a maximum amount of noise that can be allowed for solutions to exist (see the Appendix), we can define a noise parameter S as the ratio of noise to this maximum value. Calculations are done for values of S that vary between 0 and 1, corresponding to the noise-free and maximum-noise case. In our application, the noise parameter will be determined by adjusting the phase speed of the forced wave to the translation speed of the surface wind field.

Since the observed spectra are random variables, and since the wave parameters we are calculating depend very sensitively on these input values, an average over 47 frequency bands has been performed to stabilize the spectral estimates. For the frequency range of our interest, this gives a single estimate at 0.3 cycles day^{-1} with a band width of

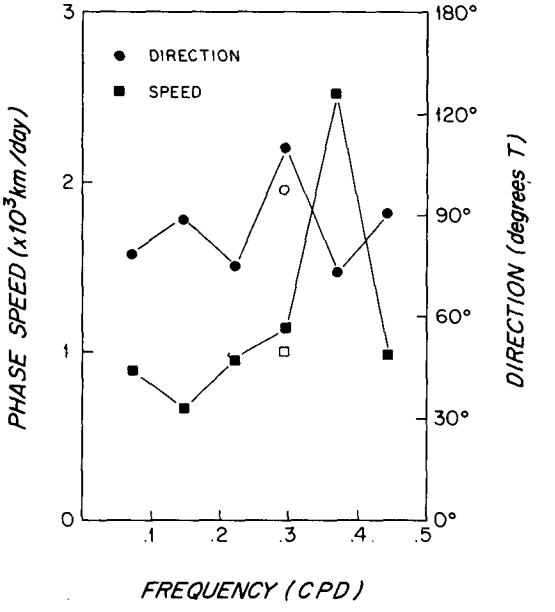

FIG. 8. Figure showing the direction (clockwise from true north, shown in circles) and the magnitude (squares) of the phase speed vector as functions of frequency. The solid and open symbols represent the calculations based on the spectral estimates averaged over 12 and 47 frequency bands, respectively.

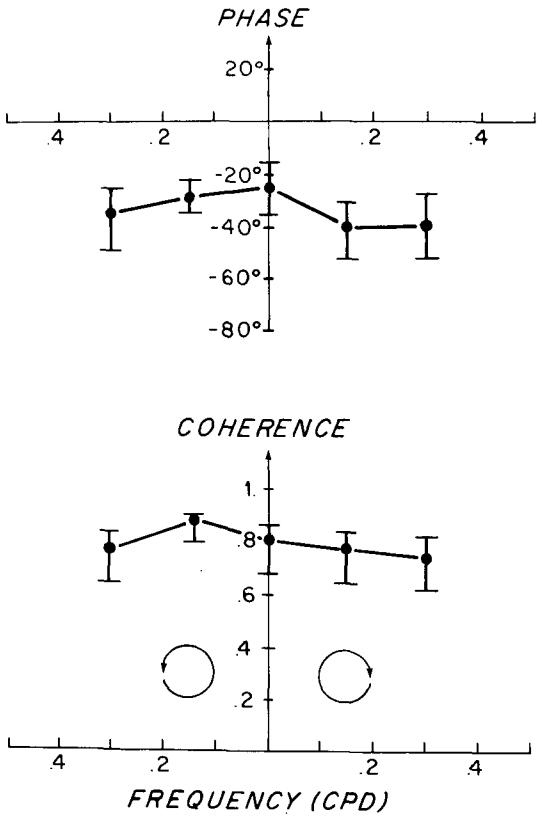

FIG. 9. Two-sided coherence and phase calculated for the current meter data at M42 and M52 during the period of 26 October 1975 to 4 April 1976. Averaging over 24 frequency bands has been performed and the error bars indicate the 95% confidence intervals.

0.3 cycles day^{-1}. The modified jackknife method (Miller, 1974) has been employed to estimate the wave parameters and their confidence intervals. By removing consecutively a single frequency band, we can calculate 47 pseudo-values defined here for any parameter θ as $\tilde{\theta}_i = n\tilde{\theta} - (n-1)\tilde{\theta}_{-i}$ $(i = 1, \ldots, n)$, where n is the total number of frequency bands used in the calculation ($n = 47$ in our case), $\tilde{\theta}$ is the parameter estimate based on the spectral values averaged over all 47 frequency bands, and $\tilde{\theta}_{-i}$ is the parameter estimate based on the spectral values averaged over the remaining 46 frequency bands when the ith band has been deleted. Except for the phase estimate, the jackknifed estimate is defined as the average of pseudo-values, and its confidence interval is determined by assuming that these pseudo-values are independent and identically distributed random variables. For the phase estimate, the method described by Batschelet (1965) has been used to determine its mean and confidence intervals. Since each phase corresponds to the direction of a unit vector in a cylindrical coordinate frame, its mean and confidence interval can be determined by the direction and magnitude of the averaged vector.

In Fig. 11, the phase lags of M52 with respect to M42 resulting from the two waves are plotted as functions of the noise parameter S. The solid dots represent the jackknifed estimates, and the shaded areas represent the 95% confidence interval. It is seen that the two waves are propagating in opposite directions, the first wave being in the direction the wind travels (i.e., upshelf), and the second wave in the direction free shelf waves propagate (i.e., downshelf). With them identified as the forced and the free wave, respectively, then the forced wave is traveling at a phase speed several times faster than the free wave. The two curves converge as S increases because the additional noise can account for more of the noncoherent motion between the two records without the large phase difference between the two waves. For the forced wave to travel at the translation speed of the wind, which was found earlier to give an 8° phase difference between M42 and M52, we estimate the noise parameter S to be 0.85. The mean phase speed of the free wave is then 526 km day^{-1}, in fair agreement with the 600 km day^{-1} phase speed Wang (1979) estimated from coastal sea level records.

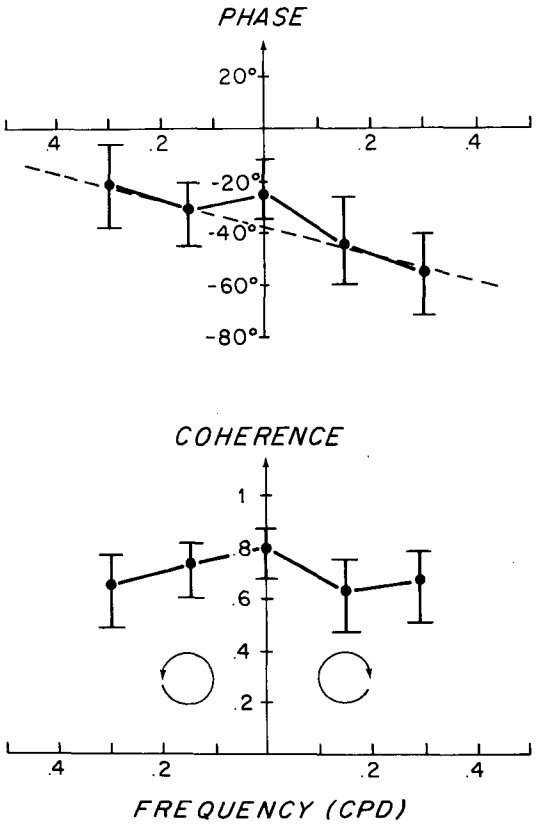

FIG. 10. As in Fig. 9, but calculated for the residual current motion after the signal that is coherent with the alongshore wind stress at EB41 has been removed. Dashed line represents a nondispersive phase speed of 816 km day^{-1}.

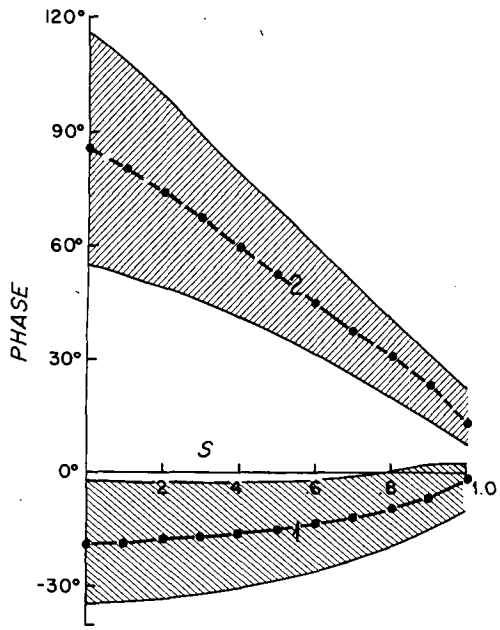

FIG. 11. The jackknifed estimate of the phase lags of M52 with respect to M42 resulting from the two waves, plotted as a function of the noise parameter S. $S = 0$ and 1 correspond to the noise-free and maximum-noise cases, respectively. The shaded areas represent the 95% confidence intervals.

We plot in Fig. 12 the rotary coefficients (Gonella, 1972) associated with the two waves. Rotary coefficient is a number that varies between the values of -1 and $+1$. The sign indicates the sense of rotation (positive for counterclockwise rotation in our convention) and the absolute value gives the ellipticity of the current ellipse. Since the first wave has a less negative rotary coefficient, the forced wave is more cyclonically polarized. Except for the limiting case of $S = 1$, when the two waves are circularly polarized (see the Appendix), the forced wave is generally more elliptical than the free wave. These results are consistent with the solutions of Buchwald and Adams (1968) and Adams and Buchwald (1969). If the first shelf-wave mode dominates, and the measurements are taken shoreward from the first zero crossing of the alongshore current, then the free shelf wave is clockwise polarized while the forced shelf wave is counterclockwise polarized when the wind field propagates upshelf. The ellipticity of the motion depends on the phase speed of the wave, and the motion is more rectilinear for the higher phase speed that is associated with the forced wave in our case. In Fig. 13, we show the partition of the total kinetic energy into the two waves and noise. Both waves make comparable contributions to the observed variance, confirming our earlier speculation. For $S = 0.85$, forced and free waves account for 41 and 39% of the total variance while the noise accounts for the remaining 20%. The uncertainties associated with these numbers are greater than that indicated by the error bars because of the additional uncertainty in estimating the noise level.

6. Discussion

For illustrative purpose, we have presented in this paper only the detailed spectral analysis of the current-meter data obtained at M42 and M52. Besides the practical consideration that M42 and M52 supply the longest overlapped data, the simple two-wave model appears to be most applicable for these two records. Since the model assumes spatial uniformity along the shelf and neglects any generation and decay of the waves, the pair of stations must be located close enough to at least show similar spectra. For the data available to us, M42 and M52 seem best to satisfy this requirement (see Fig. 4). Toward the outer shelf, the increasing influence from the deep ocean tends to invalidate this simple two-wave assumption and, expectedly, the model results become more difficult to interpret.

The loss of resolution due to heavy band averaging also presents some problems. As the spectra are red, the dynamics cannot be considered uniform over this whole band. In addition, the poor frequency resolution prevents us from examining the dispersion relation of the free-wave component, which can be compared more critically with existing

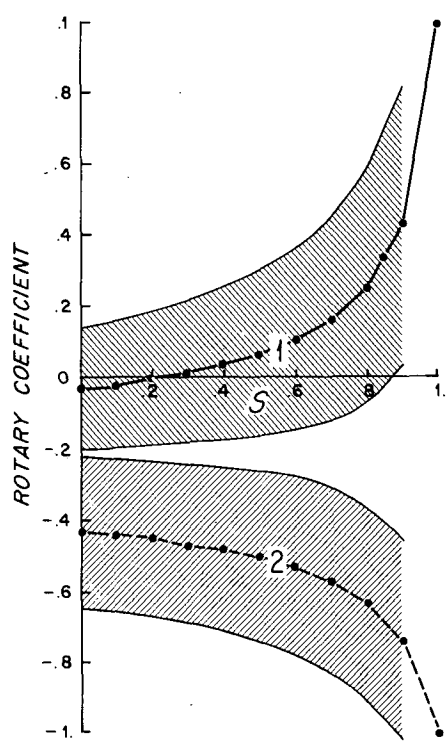

FIG. 12. The jackknifed estimate of the rotary coefficients associated with the two waves, plotted as a function of the noise parameter S. The shaded areas represent the 95% confidence intervals.

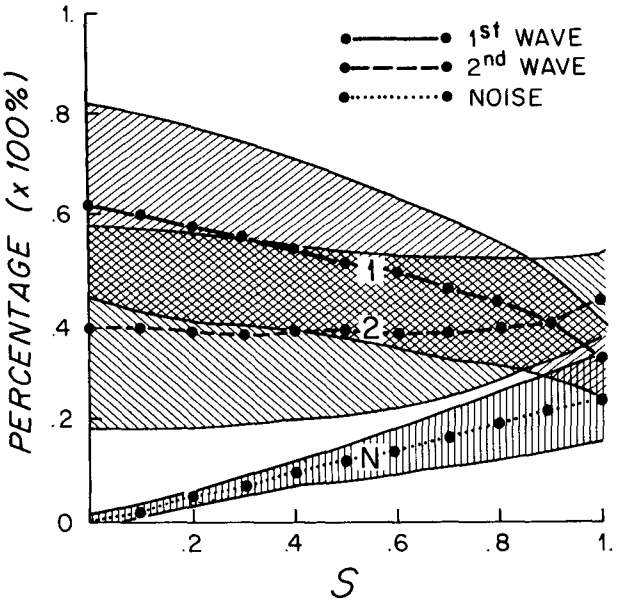

FIG. 13. The jackknifed estimate of the percentage of the total kinetic energy residing in the two waves and the noise, plotted as a function of the noise parameter S. The shaded areas represent the 95% confidence intervals.

shelf-wave theories. Since both the atmospheric and hydrographic conditions vary with season, as may the wave field, our analysis must be carried out within a time span during which the wave environment is approximately constant. Additional degrees of freedom in improving the frequency resolution can be achieved by acquiring data from the same season over several years.

Direct Eulerian current measurements are a recent advent in the Middle Atlantic Bight (Beardsley and Boicourt, 1981; Mayer *et al.*, 1979), and the search for coherent wave motions propagating along the shelf has been hampered for lack of simultaneous data along the same isobath. Our data offer a good opportunity for such a search, and this is the primary reason for choosing the current-meter data for our analysis. A similar wave analysis can be performed on coastal sea-level records which, because of their abundance, serve as a particularly attractive data base for the application of the model. The regional and seasonal variations in the wave field can be studied in a more quantitative way. However, for scalar time series, the resolution into two plane waves requires at least three stations and one has to be more careful in ensuring that the uniformity condition is approximately satisfied.

Acknowledgments. We want to thank G. R. Halliwell for supplying us with some of the wind data, and J. Vermersch, R. Limeburner, and M. Noble who helped with the initial processing of the wind and current data. We also want to thank C. Wunsch and M. Noble for some stimulating conversations, and Woollcott Smith who introduced us to the jackknife method.

H. W. Ou and R. C. Beardsley have been supported at the Woods Hole Oceanographic Institution by the National Science Foundation under Grants OCE 76-01813 and OCE 78-19513. The effort of D. Mayer has been supported by the MESA New York Bight Project. W. C. Boicourt has been supported at the Chesapeake Bay Institute by the National Science Foundation under Grants OCE 77-22774, while B. Butman's work at U.S.G.S. has been funded by U.S.G.S. and B.L.M. under contract MOOAA550-MU6-29.

APPENDIX

Two-Wave Decomposition of the Rotary Spectra

A Fourier transform of a vector time series gives an ellipse which can be decomposed into two oppositely rotating vectors (Gonella, 1972). Let $\mathbf{u}(\sigma)$ denote the vector that traces out the ellipse at frequency σ, then it can be expressed in the complex plane as

$$\mathbf{u}(\sigma) = u_c e^{i\sigma t} + u_a e^{-i\sigma t},$$

where the subscripts c and a will hereafter refer to the cyclonic (counterclockwise) and anticyclonic (clockwise) rotations. Frequently in this presentation, subscripts will be dropped to indicate the general variables. In this model, we will assume that the observed motion is a linear superposition of two plane waves propagating along the coast (x axis) and some noise, i.e.,

$$u_c = u_{1c} e^{-ik_1 x + i\varphi_1} + u_{2c} e^{-ik_2 x + i\varphi_2} + n_c,$$

$$u_a = u_{1a} e^{ik_1 x - i\varphi_1} + u_{2a} e^{-ik_2 x + i\varphi_2} + n_a,$$

where n is the noise, and the subscripts 1 and 2 will hereafter refer to the first and the second wave, respectively. Spatial uniformity in x is assumed so that the amplitudes of both waves and noise do not vary in x. Now consider the time series obtained at two locations along the coast, and let C_0 and C denote the auto- and cross-spectra of the two series; then for two uncorrelated waves,

$$\left.\begin{aligned} C_{0c} &= A_{1c} + A_{2c} + N_c \\ C_{0a} &= A_{1a} + A_{2a} + N_a \\ C_c &= A_{1c} e^{i\theta_1} + A_{2c} e^{i\theta_2} \\ C_a &= A_{1a} e^{-i\theta_1} + A_{2a} e^{-i\theta_2} \end{aligned}\right\}, \quad \text{(A1)}$$

where the A's and N's are the squares of the respective amplitudes, and θ's are the phase difference between the two series resulting from the respective waves. If the noise level is known, then (A1) forms a closed set of equations, and the amplitude and phase

of the two waves can be solved in terms of the observed spectra. To further simplify (A1), let us define, for both the rotary components,

$$R = |C|/C_0', \tag{A2}$$

where

$$C_0' = C_0 - N,$$

then (A1) reduces to

$$\left.\begin{aligned} R_c e^{i\theta_c} &= \frac{1}{1 + r_c}(e^{i\theta_1} + r_c e^{i\theta_2}) \\ R_a e^{i\theta_a} &= \frac{1}{1 + r_a}(r_a e^{-i\theta_1} + e^{-i\theta_2}) \end{aligned}\right\}, \tag{A3}$$

where θ_c and θ_a are the phases of the complex numbers C_c and C_a, and r_c and r_a are the amplitude ratios defined by

$$r_c = A_{2c}/A_{1c},$$

$$r_a = A_{1a}/A_{2a}.$$

The equations (A3) can be solved to give

$$\left.\begin{aligned} \theta_1 &= \sin^{-1}\alpha_3 + \tan^{-1}(\alpha_2/\alpha_1) \\ \theta_2 &= -2\tan^{-1}\left(\frac{\cos\theta_1 - R_a\cos\theta_a}{\sin\theta_1 + R_a\sin\theta_a}\right) - \theta_1 \\ r_c &= -\frac{R_c\cos\theta_c - \cos\theta_1}{R_c\cos\theta_c - \cos\theta_2} \\ r_a &= -\frac{R_a\cos\theta_a - \cos\theta_2}{R_a\cos\theta_a - \cos\theta_1} \end{aligned}\right\}, \tag{A4}$$

where

$$\alpha_1 = R_c\cos\theta_c - R_a\cos\theta_a,$$

$$\alpha_2 = R_c\sin\theta_c + R_a\sin\theta_a,$$

$$\alpha_3 = -R_cR_a(\alpha_1^2 + \alpha_2^2)^{-1/2}\sin(\theta_c + \theta_a).$$

The amplitudes of the two waves can be calculated by

$$\left.\begin{aligned} A_{1c} &= C_{0c}'/(1 + r_c), & A_{2a} &= C_{0a}'/(1 + r_a) \\ A_{2c} &= C_{0c}' - A_{1c}, & A_{1a} &= C_{0a}' - A_{2a} \end{aligned}\right\}$$

from which other wave properties can be calculated.

There are some trivial implications of the equations (A3). If we define (θ_1, θ_2) as the smaller of the two arcs spanned by the angles θ_1 and θ_2 in a polar coordinate system, then (θ_1, θ_2) must contain $(\theta_c, -\theta_a)$ since both r_c and r_a are positive. The two will be the same in the limiting case $R_c = R_a = 1$ when the trivial solution gives two circularly polarized waves. There is no solution when either R_c or R_a is >1. From (A2), this implies a maximum noise of

$$N_{\max} = C_0 - |C|.$$

Let $S = N/N_{\max}$ be a measure of the noise level; then S varies between the values of 0 and 1. The solution (A4) can be calculated for different values of S, corresponding to different noise levels.

REFERENCES

Adams, J. K., and V. T. Buchwald, 1969: The generation of continental shelf waves. *J. Fluid Mech.*, **35**, 815–826.

Batschelet, E., 1965: Statistical methods for the analysis of problems in animal orientation and certain biological rhythms. Amer. Inst. Biolog. Sci., Washington, DC, 57 pp.

Beardsley, R. C., and W. C. Boicourt, 1981: On estuarine and continental-shelf circulation in the Middle Atlantic Bight. *Evolution of Physical Oceanography*, B. A. Warren and C. Wunsch, Eds., The MIT Press, 198–233.

——, —— and D. V. Hansen, 1976: Physical oceanography of the Middle Atlantic Bight. *American Society for Limnology and Oceanography, Special Symposium*, **2**, 20–34.

Buchwald, V. T., and J. K. Adams, 1968: The propagation of continental shelf waves. *Proc. Roy. Soc. London*, **A305**, 235–250.

Gill, A. E., and E. Schumann, 1974: The generation of long shelf waves by the wind. *J. Phys. Oceanogr.*, **4**, 83–90.

Gonella, J., 1972: A rotary-component method for analysing meteorological and oceanographic vector time series. *Deep-Sea Res.*, **19**, 833–846.

Mayer, D. A., D. V. Hansen and D. A. Ortman, 1979: Long-term current and temperature observations on the Middle Atlantic shelf. *J. Geophys. Res.*, **84**, 1776–1792.

Miller, R. G., 1974: The jackknife—a review. *Biometrika*, **61**, 1–15.

Mooers, C. N. K., J. Fernandez-Partagas and J. F. Price, 1976: Meteorological forcing fields of the New York Bight (first year's progress report). Tech. Rep. TR76-8, Rosenstiel School of Marine and Atmospheric Science, University of Miami, 151 pp.

Noble, M., and B. Butman, 1979: Low-frequency wind-induced sea level oscillations along the east coast of North America. *J. Geophys. Res.*, **84**, 3227–3236.

Scott, J. T., and G. T. Csanady, 1976: Nearshore currents off Long Island. *J. Geophys. Res.*, **81**, 5401–5409.

Wang, D. P., 1979: Low-frequency sea level variability on the Middle Atlantic Bight. *J. Mar. Res.*, **37**, 683–697.